

Exploring size and state dynamics in CdSe quantum dots using two-dimensional electronic spectroscopy

Justin R. Caram, Haibin Zheng, Peter D. Dahlberg, Brian S. Rolczynski, Graham B. Griffin, Dmitriy S. Dolzhnikov, Dmitri V. Talapin, and Gregory S. Engel

Citation: *The Journal of Chemical Physics* **140**, 084701 (2014); doi: 10.1063/1.4865832

View online: <http://dx.doi.org/10.1063/1.4865832>

View Table of Contents: <http://scitation.aip.org/content/aip/journal/jcp/140/8?ver=pdfcov>

Published by the AIP Publishing

Articles you may be interested in

[Two-dimensional electronic spectroscopy of CdSe nanoparticles at very low pulse power](#)
J. Chem. Phys. **138**, 014705 (2013); 10.1063/1.4772465

[Stark shifts and exciton dissociation in CdSe nanoparticle grafted conjugated polymer](#)
Appl. Phys. Lett. **100**, 151908 (2012); 10.1063/1.3701719

[Spectrally resolved size-dependent third-order nonlinear optical properties of colloidal CdSe quantum dots](#)
Appl. Phys. Lett. **100**, 041102 (2012); 10.1063/1.3679381

[Optical characterization of CdSe quantum dots with metal chalcogenide ligands in solutions and solids](#)
Appl. Phys. Lett. **99**, 023106 (2011); 10.1063/1.3610456

[Spectroscopy and carrier dynamics in CdSe self-assembled quantum dots embedded in Zn_xCd_yMg_{1-x-y}Se](#)
Appl. Phys. Lett. **86**, 253113 (2005); 10.1063/1.1947909



Re-register for Table of Content Alerts

Create a profile.



Sign up today!



Exploring size and state dynamics in CdSe quantum dots using two-dimensional electronic spectroscopy

Justin R. Caram,¹ Haibin Zheng,¹ Peter D. Dahlberg,² Brian S. Rolczynski,¹ Graham B. Griffin,¹ Dmitriy S. Dolzhnikov,³ Dmitri V. Talapin,³ and Gregory S. Engel^{1,a)}

¹Department of Chemistry, The Institute for Biophysical Dynamics, and The James Franck Institute, The University of Chicago, Chicago, Illinois 60637, USA

²Graduate Program in the Biophysical Sciences, The Institute for Biophysical Dynamics, and The James Franck Institute, The University of Chicago, Chicago, Illinois 60637, USA

³Department of Chemistry and The James Franck Institute, The University of Chicago, Chicago, Illinois 60637, USA

(Received 29 October 2013; accepted 3 February 2014; published online 25 February 2014)

Development of optoelectronic technologies based on quantum dots depends on measuring, optimizing, and ultimately predicting charge carrier dynamics in the nanocrystal. In such systems, size inhomogeneity and the photoexcited population distribution among various excitonic states have distinct effects on electron and hole relaxation, which are difficult to distinguish spectroscopically. Two-dimensional electronic spectroscopy can help to untangle these effects by resolving excitation energy and subsequent nonlinear response in a single experiment. Using a filament-generated continuum as a pump and probe source, we collect two-dimensional spectra with sufficient spectral bandwidth to follow dynamics upon excitation of the lowest three optical transitions in a polydisperse ensemble of colloidal CdSe quantum dots. We first compare to prior transient absorption studies to confirm excitation-state-dependent dynamics such as increased surface-trapping upon excitation of hot electrons. Second, we demonstrate fast band-edge electron-hole pair solvation by ligand and phonon modes, as the ensemble relaxes to the photoluminescent state on a sub-picosecond time-scale. Third, we find that static disorder due to size polydispersity dominates the nonlinear response upon excitation into the hot electron manifold; this broadening mechanism stands in contrast to that of the band-edge exciton. Finally, we demonstrate excitation-energy dependent hot-carrier relaxation rates, and we describe how two-dimensional electronic spectroscopy can complement other transient nonlinear techniques. © 2014 AIP Publishing LLC. [<http://dx.doi.org/10.1063/1.4865832>]

I. INTRODUCTION

Quantum dots (QDs) have synthetically controllable structures, resulting in tunable quantum properties.^{1,2} Because of this control, QDs have been employed in a variety of imaging,^{3–5} quantum information,^{6,7} and electronic^{8,9} technologies. However, their performance in these applications is strongly affected and limited by the behavior of excited charge carriers within the nanocrystal. Charge-carrier surface trapping,^{10,11} array transport,^{12,13} multi-exciton generation,^{14–17} and recombination^{18–21} all depend critically upon ultrafast relaxation dynamics that are, in turn, influenced by parameters of excitation. Previous efforts have observed charge carrier dynamics in QDs,^{18,22–28} but broad lineshapes and ultrafast timescales complicate interpretation. New two-dimensional optical techniques with single-digit femtosecond time resolution and wavelength-specific spectral resolution can address these questions directly, providing context for prior measurements and assisting the design and implementation of future optoelectronic technologies. In this study, we apply Continuum Two-Dimensional Electronic Spectroscopy (C-2DES) to probe the ultrafast relax-

ation dynamics and nonlinear response of the lowest three electronic transitions in 3.0 ± 0.3 nm radius CdSe QDs. C-2DES utilizes filament-generated white light to combine the simultaneous temporal and spectral resolving power of 2D spectroscopy^{29–31} with the large bandwidth, stability, and multi-state resolution of continuum-probe transient absorption (TA) spectroscopy.³²

To probe QD dynamics in nanocrystals, various optical techniques have been used. Some methods probe the dynamics of charge carriers and formation of biexcitons, in particular TA,^{30–32,34} (including state-selective^{21,25,26,28,33} and intraband^{24,34–36} methods) and transient photoluminescent studies.^{37,38} These techniques illuminate relaxation dynamics with great accuracy, but can convolve contributions from many sources of disorder in nanocrystals, precluding a detailed understanding of the distinct roles of static disorder, such as size polydispersity, and dynamic disorder, such as coupling to the environment. Other methods successfully probe fluctuations and inhomogeneity including photon echo peak shift experiments,^{39–41} hole-burning,^{22,42} and 2DES^{40,43–46} but have been focused on the band edge or two lowest-lying excitonic states, for which the dynamics correspond mainly to hole relaxation. Recent 2DES work with broadband pulses on smaller dots by Turner *et al.*⁴⁴ demonstrate electronic coherence between the two lowest lying

^{a)}Author to whom correspondence should be addressed. Electronic mail: gsengel@uchicago.edu

excited states. Griffin *et al.*⁴⁵ used similar 2DES measurements to show that hole relaxation proceeds on the same time scale as the electronic coherence, challenging Turner *et al.*'s assignment of excitonic coherence. Finally, several theoretical studies have shown how 2DES should be able to probe size-dependent phonon couplings within a polydisperse sample.^{47,48} This work examines larger dots than Turner *et al.*⁴⁴ and Griffin *et al.*⁴⁵ (band-edge at ~ 1.95 eV, compared to 2.05 eV). For this reason, the excitons are more closely spaced in energy, allowing broadband excitation to address a larger range of transitions simultaneously, while also having significant spectral coverage of the PL emission energy, which causes significant differences in reported 2D spectra. In our work, we resolve clear differences in the nonlinear response depending strongly on excitation energy. This study focuses on the character and dynamics of spectral features resulting from excitation into the $|X_1\rangle$ and $|X_3\rangle$ manifolds, which differ by the electronic state excited. Our 2DES experiments confirm previous TA results and reveal new information about excitation dependent lineshape and charge carrier relaxation to the band-edge, and subsequently to the PL state. Coherent electronic dynamics are the focus of a separate paper.⁴⁹

The main advantage of C-2DES for our study is that it reports dynamics as a function of the specific excitation energy (coherence energy). We present several results and conclusions: (1) We connect 2D measurements to previous state-selective transient absorption work. (2) We show that hot exciton cooling processes lead to increased signatures of surface trapping, in accordance with recent literature. (3) We measure ultrafast fluctuations, oscillations, and relaxation of the band-edge exciton to the photoluminescent state, manifesting as peak shape change and peak shift. (4) We find clear signatures of size-dependent polydispersity in the nonlinear response upon excitation of hot electrons. And (5) we show that the rate of electron relaxation strongly depends on excitation. The ability to measure many of these features simultaneously exemplifies the utility of C-2DES as a technique for screening the behavior of QD samples.

A. Excitonic structure of quantum dots

CdSe QD electronic structure has been described with varying levels of theory.^{42,50,51} In the simplest picture, quantum confinement of charge carriers creates discrete electron and hole excited states near the band-edge. Optical excitation of a QD promotes an electron (e) to the conduction band, leaving a corresponding hole (h) in the valence band. Colloidal QD absorption spectra thus display distinguishable features, which can be described by the electron and hole state populated. These states are labeled by a principal quantum number and an angular momentum state accordingly (e.g., 1S, 2S, 1P, 1D), and a total angular momentum term (e.g., 3/2, 1/2). Figure 1(a) shows the first four hole and two electronic states. Due to selection rules, only certain allowed electron hole-pairs (excitons) are created upon excitation. We label these states according to previous convention.^{21,44} The two lowest energy excitons, $|X_1\rangle$ and $|X_2\rangle$, correspond to

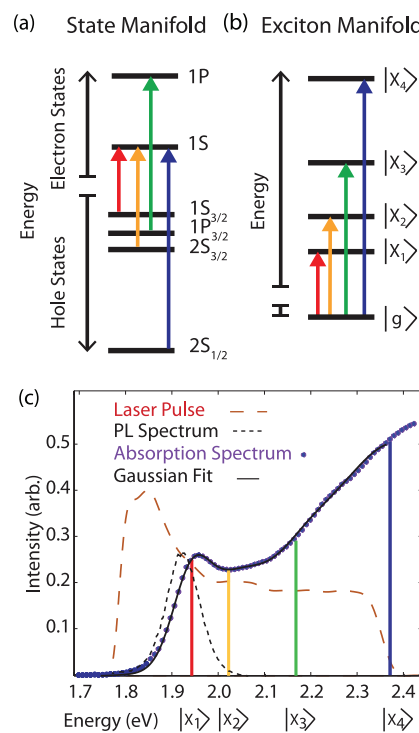


FIG. 1. (a) The manifold of hole and electron states that form the excitons probed in this experiment (names derived from the multiband effective mass approximation method).⁴² Upon excitation these states form. (b) Four weakly bound electron-hole pairs, labeled $|X_1\rangle$ to $|X_4\rangle$. (c) The ultrafast pulse spectrum used to interrogate the system is plotted with the absorption spectrum of zinc-blende CdSe QDs ($r = 3.0 \pm 0.3$ nm). The center positions of a five Gaussian fit are indicated in orange, yellow, green, and blue vertical lines, in good agreement with previous work for dots this size.²³ Reprinted with permission from Caram *et al.*, J. Phys. Chem. Lett. 5, 196 (2013). Copyright 2013 American Chemical Society.

$1S_{3/2}(h) \rightarrow 1S(e)$ and $2S_{3/2}(h) \rightarrow 1S(e)$, respectively. $|X_3\rangle$ corresponds to $1P_{3/2}(h) \rightarrow 1P(e)$, states which differ in both hole and conduction bands. The fourth, $2S_{1/2} \rightarrow 1S(e)$, represents a split-off band. In Figure 1(b), we illustrate these states forming the four lowest energy excitonic states.

In this study, we probe the multiple excitonic states in a single ensemble of zinc blende quantum dots ($r = 3.0 \pm 0.3$ nm). We show a transmission electron micrograph, an x-ray diffraction spectrum, and a histogram displaying the size-distribution in Figures S1(a)–S1(c) in the supplementary material.⁵² Figure 1(c) shows the room-temperature, ground-state absorption spectrum of our QD sample. Based on previous assignments,^{23,53} we fit a five-Gaussian function for $|X_1\rangle$ through $|X_5\rangle$, corresponding to the approximate transition energies of the five lowest energy excitons, with good agreement to reported parameters for QDs of this average size.^{23,54} In this preparation of quantum dots, the two lowest energy excitons are not well-resolved in the linear absorption spectrum due to the small energy difference between states and $\sim 10\%$ radial polydispersity. We thus focus mostly on the dynamics of the band-edge exciton ($|X_1\rangle$) and the well-separated $1P_{3/2}(h) \rightarrow 1P(e)$, state ($|X_3\rangle$). We also plot the photoluminescence (PL) laser pulse spectrum, showing near uniform overlap with the spectral response of the system (Figure 1(c)). The fifth transition is centered outside the laser bandwidth and thus is not excited.

B. Femtosecond nonlinear spectroscopy of quantum dots

Valence and conduction (photexcited electron and hole) bands each exhibit different densities of states near the band edge, allowing the respective charge carriers to undergo different relaxation pathways.⁴² In the hole (valence) manifold of CdSe QDs, the close energy spacing of the states permits fast relaxation via coupling to ligand, acoustic, and optical phonon modes.^{24,25,32,39,42,55–58} Electron-hole correlated processes play a larger role in electron relaxation than in hole relaxation both due to the sparser density of states for electrons near the band edge, as well as due to angular momentum considerations. For example, electrons have been reported to relax via an Auger-like mechanism,^{19,32,56,59} in which electron-hole wavefunction overlap allows electrons to transition while simultaneously exciting a hole in the valence band. This process is thought to occur due to anomalously fast band-edge relaxation for these states, not permissible via phonon or acoustic modes, as well as size dependent studies which shows faster decay with smaller particles, a function of increased electron/hole wave function overlap.^{21,25,26,36,59}

Within an ensemble of colloidal QDs, size and shape polydispersity creates a range of possible transitions in the electron and hole manifolds, broadening all features. To understand and control charge carriers, we must spectroscopically distinguish the exciton states and their corresponding dynamics. However, resolving these states with time-resolved absorption and fluorescence spectroscopies is confounded by inhomogeneous broadening from finite nanocrystal size distributions and excitation into mixed-character excited states, which obscure and convolve transient features even in the most monodisperse nanocrystal preparations.

To model the role of size inhomogeneity on absorption linewidth, we consider the excitation using the particle-in-a-sphere potential.⁵¹ This approach is suitable for the first three optical transitions but neglects valence and conduction band mixing and angular momentum, which must be treated using more detailed models.^{50,60} In this simple approach, the energies of the optical transitions, E , are approximately proportional to $1/r^2$, where r is the QD radius. For simplicity, we assume a Gaussian distribution of radii to derive a state-dependent inhomogeneous lineshape. These approximations result in a skewed Gaussian profile for energies represented with the following equation:

$$P(E) = \exp\left(-\frac{r_0^2(\sqrt{\Delta E_a/E} - 1)^2}{2\sigma^2}\right), \quad (1)$$

where r_0 and σ are the mean and the standard deviation of the particle radius distribution, respectively, and ΔE_a is the difference between the exciton energy and the band-gap energy. For this size distribution, the full width at half maximum (FWHM) is both state- and size-dependent and is given by

$$FWHM = 2\sqrt{2\log 2} \frac{2\Delta E_a a_0^3 \sigma}{(a_0^2 - 2\log(2)\sigma^2)^2}, \quad (2)$$

which is similar to an expression derived by Klimov.⁵³ The important aspect of this distribution is that the degree of inho-

mogeneity depends on both the *polydispersity* of the sample and the *energy* of the individual excited state relative to the band gap. In QDs, this simple relationship implies that radial inhomogeneity will result in broader lineshapes for higher energy exciton states. Furthermore, at higher energies, the states become completely overlapped, not permitting direct excitation to a specific manifold. Figure S1(d) in the supplementary material⁵² shows Eq. (1) for the first three states for the size distribution used in this study, illustrating the differential inhomogeneous linewidths for the first three excitonic states.

We employ 2DES to study the three lowest energy exciton states in an ensemble of QDs. 2DES excels at probing coherent and incoherent dynamics in spectrally inhomogeneous systems.³¹ The origin of features in 2DES can best be explained using perturbation theory, with each term of the perturbative expansion represented by a double-sided Feynman diagram. Three electric fields act on the sample in sequence, with time differences denoted τ , T , and t . Each Feynman diagram illustrates how these resonant electric field interactions yield excited and ground state populations and coherences within the density matrix formalism. Figure 2 illustrates diagrams that can be used to explain spectral features in 2D experiments. For simplicity, we only show rephasing diagrams ($\tau > 0$), though this study focuses on combined 2D spectra which include both rephasing and nonrephasing pathways, for comparison to previous TA work.^{30,61} There are several different signals which give rise to features in 2DES. Ground state bleach (GSB) results from system evolution in the ground state during T , while stimulated emission (SE) results from system evolution on the excited state prior to electron-hole recombination. The third, excited state absorption (ESA), arises from excitation of a second electron-hole

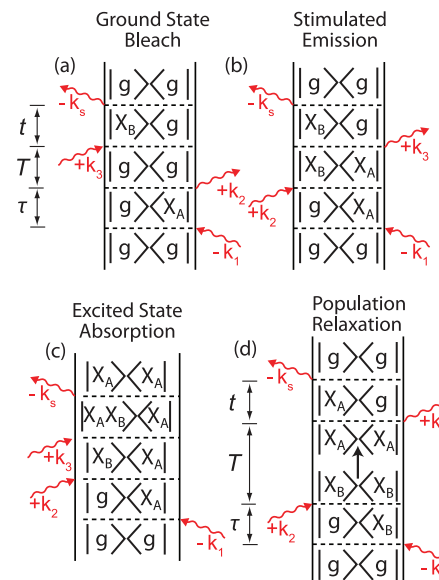


FIG. 2. Double-sided Feynman diagrams for the rephasing ($\tau > 0$) signal in 2DES of QDs. Each red arrow represents an electric field interaction, which perturbs the system and puts it into a population or coherent state of the density matrix for the time period specified on the top left. For (a) and (b), when $|X_A\rangle = |X_B\rangle$, the signal appears on the diagonal of the 2D spectrum. If $|X_A\rangle \neq |X_B\rangle$ the signal appears on a cross-peak. For both cases, a signal arising from pathway (c) will result in a negative signal in a position shifted by the biexciton binding energy. Pathway (d) represents energy transfer, which also yields cross-peaks off the diagonal.

pair by the third pulse. By convention, GSB and SE are positive signals, while ESA is negative. During electron and hole relaxation to the band-edge, SE and ESA cross-peak signals will grow during the waiting time while the GSB signal remains static, as shown by the population relaxation Feynman diagram (Figure 2(d)). Due to broadband excitation, additional pathways involving coherences between excited states, contribute to the signal when state $|X_a\rangle \neq |X_b\rangle$. Electronic coherences may contribute strongly to the early time ($T < 200$ fs) signal,⁴⁴ while vibrational/phonon coherences periodically modulate the signal for picoseconds.^{57,58} Furthermore, various mixed-biexcitonic states are possible, especially at early times prior to charge carrier relaxation to the band-edge.^{33,40}

II. EXPERIMENTAL METHODS

A. Continuum two-dimensional electronic spectroscopy

Many excellent reviews extensively discuss the implementation of broadband 2DES.^{31,62–66} In brief, three laser pulses are focused to a common point in the sample and a signal field is emitted in a unique phase-matched direction ($k_s = -k_1 + k_2 + k_3$). The time separation between the first two pulses (the coherence time, τ) puts the system into an optical superposition between the ground and excited states. After interaction with the second pulse, the system evolves on the excited or ground state, or in a coherence between excited electronic or vibrational states for a waiting time, T . The third pulse puts the system into a second optical coherence from which a signal is emitted in a phase-matched direction after a time t .

Continuum 2DES extends this technique by introducing filament generated “white light” as a laser source to traditional 2DES. This source generates similar bandwidth to the broadest implementation of non-collinear optical parametric amplification used in broadband 2DES.^{44,66} To generate continuum, we focus the 4 W, 5 kHz, 38 fs FWHM output beam of a Legend Elite Ti:sapphire regenerative amplifier (Coherent Systems, Inc.) into 2 atm argon gas, producing 450–900 nm pulses (stability 0.4% SD/mean, measured at 10 Hz). We then select a portion of the continuum (525–700 nm) and temporally compress it using the Multiphoton Intrapulse Interference Phase Scan (MIIPS) method⁶⁷ with instrumentation from Biophotonics Solutions. Using TG-FROG and MIIPS autocorrelation (Figures S2(a) and S2(b) in the supplementary material),⁵² we measure a pulse durations of ~8–10 fs. C-2DES addresses the enhanced nonlinear dispersion that affects such broadband pulses by using an all-reflective redesign of the 2DES system to collect distortion-free, spectrally broad 2D spectra (Figure S2 in the supplementary material).⁵² We employ angled, motorized delay stages to generate precise sub-fs optical delays (further experimental details of the apparatus are in the supplementary material including Figure S2).⁵² Each delay stage is calibrated using spectral interferometry.⁶⁸

This signal field is then heterodyned with a reference pulse (set ~1 ps after beam 3 and attenuated three orders of

magnitude) and detected and frequency resolved with a commercial Shamrock spectrometer and Newton camera (Andor Technology, Inc.). At each τ , we collect an interferogram on the camera in ω_t , as well as several reference signals for scatter subtraction. We generate an individual 2D spectrum by scanning beams 1 and 2 from –60 to 80 fs in steps of 1 fs for each waiting time T , producing spectra from 0 to 1000 fs in steps of 5 fs. To generate a 2D spectrum, we first Fourier transform over ω_t to create a t vs τ plot. We then apodize the signal in the t domain with a 300 fs window function to eliminate scatter and homodyne components. To generate the final ω_t vs ω_τ plot, we Fourier transform over both domains, zero-padding by a factor of 2 in the ω_τ domain. The $\hbar\omega_\tau$ axis is the coherence energy axis, and represents where the system absorbed light, while the $\hbar\omega_t$ axis the probe axis, which describes the fate of that excitation. The experiment was repeated several times with very similar results (Figure S6 in the supplementary material). Solvent-only spectra were taken for comparison, contributing 10% of the signal at $T = 0$, and negligible signal by $T = 20$ fs. To avoid non-resonant solvent signals, all analysis is performed for signals after the first 20 fs. Photon flux is adjusted such that fewer than 0.3 excitations per QD are expected, implying that the experiment operates predominantly in the single exciton manifold (14 nJ/pulse, 100 μm diameter beamwaist, and sample OD of 0.3 at 630 nm).^{43,53} Control experiments with 2× higher power (Figure S3 in the supplementary material)⁵² show no visible differences indicating that we are observing minimal multi-exciton effects. Zinc-blende CdSe QDs were synthesized following the procedure established by Chen *et al.*⁵⁴ Size and crystallinity of the QD samples was examined using transmission electron microscopy and powder x-ray diffraction. More information is provided in the supplementary material and Figure S1.⁵²

B. Phasing to pump-probe

After scatter subtraction and Fourier windowing, each individual spectrum is phased to separately collected broadband pump-broadband probe data.⁶⁴ Phasing enables the assignment of the sign of peaks in 2D spectra to ESA, GSB, and SE pathways, as understood in TA literature. Spectrally resolved continuum-pump continuum-probe spectra were collected for each waiting time. The 5 kHz pump beam was chopped at 2.5 kHz, and pump-probe and probe-only spectra were collected on a high-speed line scan camera (Horiba). TA spectra were acquired for all time delays corresponding to the waiting times of the 2D spectra. Applying the projection-slice theorem, we fit the projection of the real part of the 2D spectrum onto the ω_t axis to the TA spectrum⁶⁹ using

$$PP(T, \omega_t) = \text{Re} \left\{ A \int_{-\infty}^{\infty} S_{2D}(\omega_\tau, T, \omega_t) \exp(i\phi + i(\omega_t - \omega_0)t_c + i(\omega_t - \omega_0)^2 t_q^2 + i(\omega_\tau - \omega_0)\tau_c) d\tau \right\}, \quad (3)$$

where A , ϕ_c , t_c , t_q , and τ_c are slight corrections to the measured timings and phase between each electric field. We show

the results of a typical fit in Figure S4 in the supplementary material.⁵²

III. RESULTS AND DISCUSSION

A. Features in 2D spectra of QDs

In Figure 3(a), we show a sequence of two-dimensional spectra taken at $T = 20, 80$, and 600 fs. In the supplementary material,⁵² we include a movie of the data to show the overall dynamics. 2D spectra of QDs show several unusual features, not commonly observed in 2D spectra of molecules and supramolecular complexes. QDs do not show a strong permanent signal on the diagonal at early times. Instead, signatures of ESA strongly modulate the observed lineshapes. At early times, the signal appears more structured as mixed higher energy biexcitons and electronic coherent signatures contribute to the signal.^{33,46} As time progresses, the excitons quickly relax to the band-edge, resulting in more static lineshapes. Furthermore, due to continuous absorption above the band-edge, the signal appears spread across both the coherence energy and probe dimensions, rather than in clearly definable diagonal peaks and cross-peaks, especially at longer waiting times. Fast relaxation also broadens lineshapes along the coherence frequency dimension.

To understand these spectra, we turn to the large body of transient absorption literature studying QD dynamics, sig-

nals, and lineshapes as well as to more recent work using 2DES. In Figure 3(b), we illustrate the connection between 2DES and state-resolved, TA spectroscopy, as explicated by several groups.^{29,30,44,61,70} Both 2DES and TA explore the same nonlinear processes. In the pump-probe experiment, the pump pulse initiates dynamics for a specific state (via narrowband excitation), and a probe pulse interrogates the nonlinear response of the system after a certain time, generating a one-dimensional spectrum for each delay. 2DES utilizes two broadband pump pulses, which together encode the optical frequency of excitation into the sample as demonstrated in the Feynman diagrams shown in Figure 2. 2D spectra are collected at different waiting time delays, tracking charge carrier relaxation via changes in signal amplitude. In a 2D spectrum, cuts, or slices, through the spectrum at specified coherence energies represent a similar signal to a single transient absorption spectrum for a given value of T and a given narrowband input (a “pseudo TA spectrum”). Therefore, a series of slices at specified times resolve the dynamics of a specific state or sub-ensemble. As can be seen in Figure 3, aspects of the nonlinear response vary significantly depending on the coherence energy. This simple “pump-probe” interpretation of 2DES is sufficient for consideration of charge-carrier relaxation in 2D spectra of colloidal QDs, although it neglects oscillatory contributions to the spectra from coherent dynamics invisible to state-resolved, pump-probe experiments as discussed above.⁷¹ We illustrate how these features can be compared to previous TA work and notation in Figure S5 of

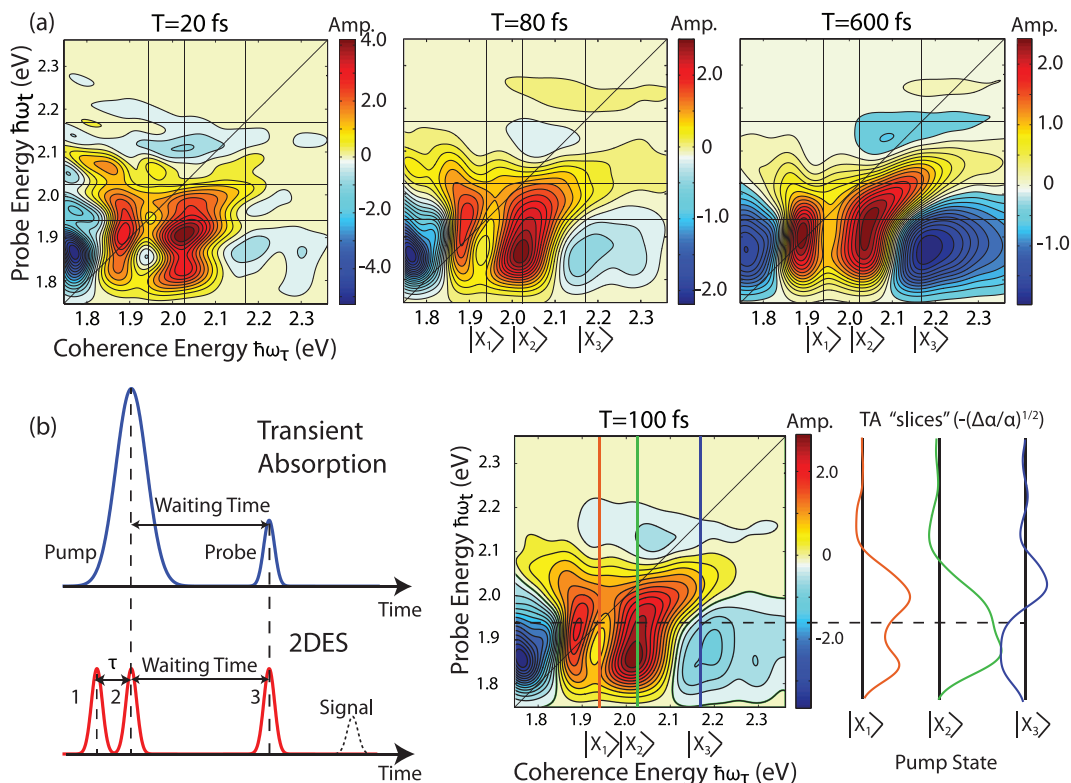


FIG. 3. (a) A time progression of 2D electronic spectra illustrating the evolution of features over time. At early times, the 2D spectrum shows several distinct features and decreased amplitude at higher energy excitation. As time progresses, the features become smoother, as the system relaxes to the band-edge, with very little change after 500 fs (movie in supplemental information⁵²). (b) The pulse sequences for pump-probe and 2D spectroscopy are diagrammed, showing the analogous time delays. (c) A 2D spectrum from which pseudo transient absorption slices can be extracted for $T = 100$ fs by plotting the signal for a specific coherence energy. The dotted line represents the position of the peak of the photoluminescent state. Depending on the initial state excited, different positive and negative features appear below the PL state.

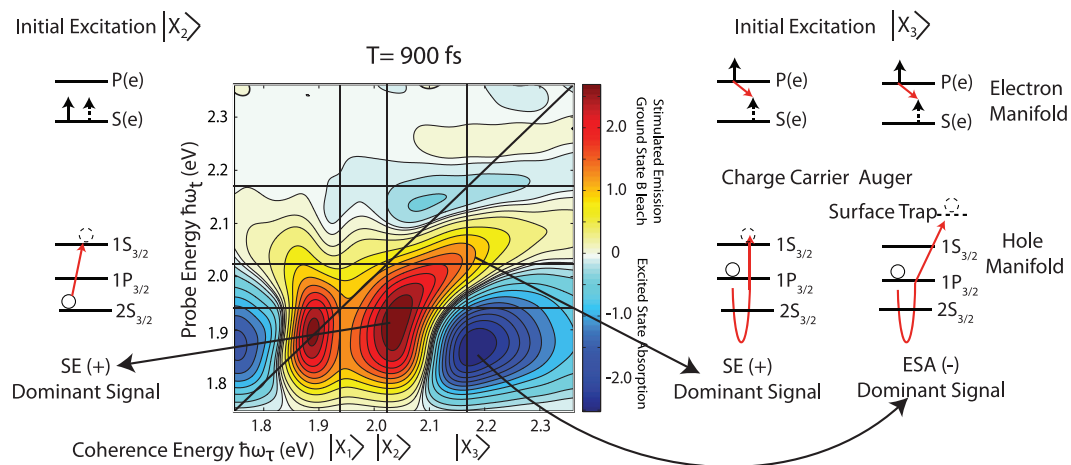


FIG. 4. Explanation of the origin of positive and negative features at $T = 900$ fs, after excitonic relaxation to the band-edge. Half arrows represent electrons, while circles represent holes. “Dotted” electrons and holes represent the final state of the charge carrier. Red arrows represent the relaxation process. The change in response between different input energies illustrates the dynamic relaxation processes from $|X_2\rangle$ and $|X_3\rangle$ to the band edge. For $|X_2\rangle$, hole relaxation proceeds quickly and outcompetes surface trapping. Excitation into $|X_3\rangle$ results in more highly excited holes after electron relaxation, which can either relax to the band edge, resulting mostly in stimulated emission, or can be trapped at the surface, which results in more excited state absorption (creation of second electron-hole pair by the probe beam).

the supplementary material.⁵² Coherent dynamics are the subject of a separate publication.⁴⁹

The primary difference between different TA “slices” upon relaxation to the band-edge (completed in <1 ps)^{13,32,35,59} appears at and below $|X_1\rangle$ (~ 1.93 eV). Figure 3(b) illustrates that initial excitation into $|X_1\rangle$ and $|X_2\rangle$ yield a positive GSB and SE nonlinear response. Excitation into $|X_3\rangle$ shows a negative signature below the band-edge, overlapping the spectral location of the PL state. In Figure 4, we explicate the origin of this change in nonlinear response following the scheme proposed by Sewall *et al.*³³ Hot electrons (excitation into $|X_3\rangle$) relax via an Auger-like mechanism, with electrons transferring energy to holes. This relaxation yields a highly excited hole state which subsequently relaxes through its manifold to the band edge. During this relaxation, surface trapping can compete with relaxation to the band-edge. A surface-trapped exciton has a weak oscillator strength,⁷² reducing the stimulated emission pathway compared to the ESA pathway. ESA yields a negative signal at and below the band-edge due to the biexciton binding energy.⁷³ Some excited holes can reach the band-edge during this time, creating a stimulated emission peak that outcompetes the ESA signal at higher probe energies. Initial excitation into $|X_1\rangle$ and $|X_2\rangle$ relax quickly to the band-edge showing less surface trapping, and thus present mostly positive signatures at and below the band-edge. We cannot estimate the biexciton binding energy because the 2D signal is partially convolved with the laser pulse spectra, which peaks in the red part of the spectrum yielding stronger signals in that region. However, it appears that at higher excitation energies, the relative difference between the locations of the band-edge SE peak and of the ESA peak grows in magnitude, suggesting differential binding energy within the ensemble of QDs.

Resolution of the coherence energy (“pump” energy) illustrates that initial excitation into $|X_3\rangle$ yields a consistently negative feature below the band-edge in this particular QD en-

semble. As the excitation transitions from primarily excitation of $|X_1\rangle$ and $|X_2\rangle$ to $|X_3\rangle$, this negative feature grows in, conclusively showing a crucial state-dependent difference in the nonlinear response. Better surface passivation or more uniform structures may minimize relaxation through this pathway. Furthermore, recent work on aged CdTe QDs has shown long-lived ESA below the band-edge signatures indicative of increased surface trapping.⁷⁴ This ESA feature is implicated as the primary challenge for creation of efficient QD lasing materials^{10,18} and is clearly resolved in C-2DES spectra only upon excitation into higher lying electronic states.

B. Lineshape changes of the band-edge exciton

2DES resolves 2D lineshapes, which indicate different sources of excitonic disorder. Diagonally elongated lineshapes indicate correlation between coherence and probe energy, i.e., inhomogeneous broadening. In contrast, round, symmetric lineshapes indicate energetic fluctuations that occur during T , which result in a “loss of memory” of the energy of the excitation.³¹ We observe distinct spectral signatures of inhomogeneity depending on the energy of excitation. Figure 5(a) shows a C-2DES spectrum from waiting time $T = 1000$ fs, after hot excitons have relaxed to the emissive state.^{21,53} The slope of a feature and its dynamics report on the interaction of that state with its environment. A persistent diagonal slope demonstrates static disorder, which is usually attributed to size polydispersity in QDs. Features that change in slope as waiting time advances indicate the presence of dynamic disorder, where a spectral feature evolves from a diagonally elongated shape to a rounder shape over time as the exciton samples more configurations of the local environment. In the supplementary material,⁵² we include a movie of the progression of two-dimensional spectra, emphasizing the band-edge feature $|X_1\rangle$ and the $|X_3\rangle/|X_1\rangle$ cross-peak feature.

In Figure 5(b), we focus on the change in slope of the band-edge feature as highlighted in Figure 5(a). Fast

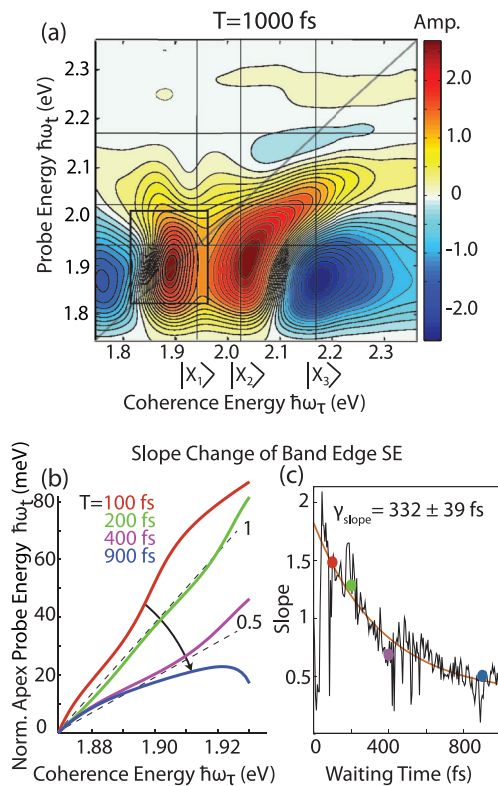


FIG. 5. (a) 2D spectrum of CdSe QDs taken at $T = 1000$ fs. (b) We plot the position of the vertical apex of the band edge feature for several waiting times as described in the text. The change in the slope of this feature represents different processes that introduce static and dynamic disorder into the QD ensemble. To better show the change of slope, we subtract the minimum probe energy for each feature. (c) The slope of the band-edge exciton starts with a slope greater than 1 and relaxes to an equilibrium value estimated to be ~ 0.5 with an exponential time constant of 332 ± 39 fs, indicating ligand/phonon solvation of the band edge exciton as it relaxes to the PL state. The slope change is a direct measure of peak shape change as the system loses memory of its initial excitation.

processes involving solvation and phonon excitation dominate the dynamics governing relaxation of the band-edge exciton $|X_1\rangle$, and have been extensively characterized.^{25,42,45} To extract the slope of $|X_1\rangle$, we find the frequency of the apex of the feature along the probe energy domain, $\hbar\omega_t$, for a range of coherence energies $\hbar\omega_\tau$, within the inhomogeneous linewidth of $|X_1\rangle$ as defined by Eq. (2). We then plot the extracted feature apex for a range of waiting times to quantify the peak shape change in analogy to the center line slope method from 2D infrared spectroscopy.⁷⁵ Fast spectral diffusion processes cause the peak slope to evolve from an initially diagonally elongated lineshape (slope > 1) to a value of 0.5 over the first picosecond. In Figure 5(c), we plot the total slope of the feature as a function of waiting time. Fitting to a single exponential starting at $T = 40$ fs (after large initial oscillation), we observe that relaxation occurs in 332 ± 39 fs, indicating rapid loss of memory of the initial excitation in the band-edge exciton. This relaxation process is slightly slower than previous photon echo peak shift results which measured the exponential lifetime of the relaxation to be on the order of 150–200 fs, with other faster components, though these methods did not span the photoluminescent state.^{39,41} The lack of persistent diagonal elongation in this peak shows that dynamics of the transition to the emissive state from $|X_1\rangle$ are not strongly size

dependent and are driven by dynamic disorder. Environmental fluctuations on a sub-picosecond time scale cause considerable energetic fluctuations of the band-edge exciton. Possible sources of this dynamic disorder include coupling to optical and acoustic phonon modes, coupling to vibrational modes of surface ligands, and solvent polarization. Further experiments varying these parameters are needed to conclusively assign the origin of the dynamic disorder.

The dynamics of $|X_1\rangle$ are shown in greater detail in Figure 6. The slope change indicates dynamic broadening of the peak, i.e., loss of memory of the excitation energy. At the same time, energetic relaxation also manifests as the peak shifts downward in an excitation-dependent manner. To describe this process, we use the term “solvation,” when the environment (solvent, ligands, phonons) interacts with the transition dipole created by the new electron-hole pair. To illustrate the solvation of exciton $|X_1\rangle$, we examine the apex probe energy (the line traced out by plotting the energy of the apex of each vertical slice through the feature) for several waiting times over this feature in Figure 6(a). In Figure 6(b), we show all of the apex probe energies for this feature, which illustrate several different peak shape and position changes. In Fig. 6(c), we highlight the downward frequency shift of this peak for several values of coherence energy, $\hbar\omega_\tau$, demonstrating that the rate of solvation correlates to the coherence energy. The blue edge of the exciton decays to its equilibrium value at half the rate of the central part (251 fs compared to 133 fs, as shown in Figure 6(b)). The total shift (estimated from the middle of the feature) is approximately 20 meV, in good agreement with the shift between the center of the band edge exciton $|X_1\rangle$ and the peak of the PL state. We therefore assign the final relaxed state as the PL state. Furthermore, we observe the presence of an oscillatory signal on the red-edge of the feature. We plot the oscillation and its Fourier transform in Figure 6(d). The dominant frequency observed is that of the LO phonon mode at 208 cm^{-1} . The oscillatory signal provides further experimental evidence that the LO phonon mode modulates the frequency of excitation, rather than the amplitude, as discussed in Sagar *et al.*⁵⁸ This oscillation indicates that the phonon mode modulates the energy gap between ground and excited state, rather than the strength of the transition (via non-Condon coupling between vibration and transition dipole). Energy fluctuations (as measured by the change in slope) and total reorganization (as measured by the frequency shift) are consistent with a fast environmental response to excitation into $|X_1\rangle$.

The dynamics of the PL state are crucially important for optical applications of QDs. Interestingly, we observe that despite our polydisperse sample, the dynamics of the PL state are determined by fast, homogeneous broadening processes. Such processes are evident in the combination of a downward energy shift and slope change in the band-edge exciton feature, which indicate dynamic “solvation.” The red edge of the PL signal includes large members of the QD ensemble and small particles in favorable (low energy) “solvation” environments. The blue edge contains small QDs and large particles in high energy solvent configurations. As time progresses, the ensemble of QDs sample more environments, broadening the peak which manifests as a slope change. However, the overall

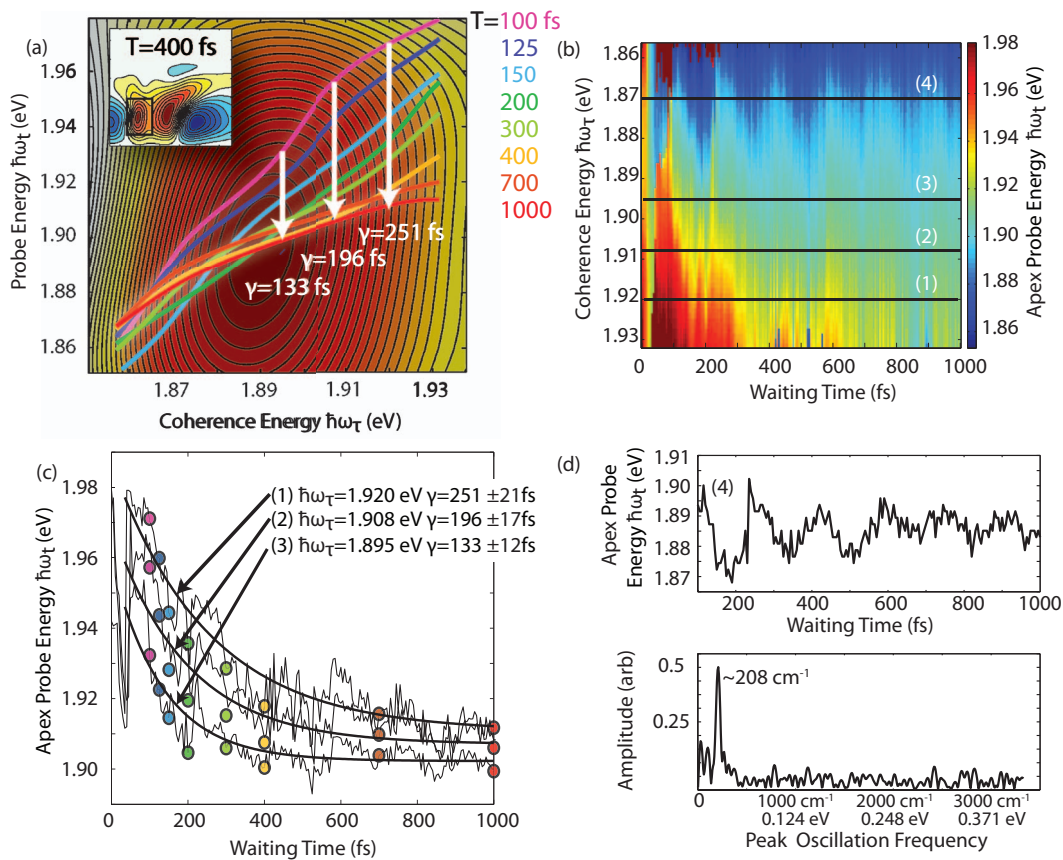


FIG. 6. (a) Apex probe energy from the band-edge plotted for different waiting times superimposed on the feature at 400 fs. Waiting times are color-coded and indicated on the right side of the figure. The white arrows represent the relaxation of the feature for a given input energy. (b) The full matrix of apex probe energies for the band-edge exciton reported in Figure 5 illustrates the lineshape change during waiting time. One can see a large difference between waiting times, and across different coherence energies. (c) Traces taken from the lines 1–3 are shown in (b), which represent the frequency shift for different input coherence energies. Colored dots represent the points corresponding to the colored curves in part (a). Each trace shown is fit to single exponential, starting at 40 fs, illustrating that different rates of energetic relaxation arise depending on the initial solvation environment. The middle of the feature relaxes a total of ~ 20 meV with a lifetime of 133 fs, indicating fast solvation via phonon and ligand modes. (d) Trace 4, from the red edge of this feature demonstrates clear oscillation which indicates modulation in the peak location by phonon modes. Below, the power spectrum resulting from the Fourier transform of the trace shown, showing the longitudinal optical phonon frequency (208 cm^{-1}).

downward shift shows that upon excitation, the environment responds to the excited state environment (the charge distribution) leading to the red-shifted PL state. Such a response is, in essence, a Stokes shift. Because of this dynamic disorder, QD samples have narrow optical gain profiles in the band edge exciton despite size inhomogeneity. Tuning the coupling strength to solvent coordinates has already been accomplished via the development of core-shell materials and the implementation of surface passivation.^{36,76} Controlling dynamic response may facilitate the development of new optoelectronic properties for QD samples, such as tuning the laser gain or creating quantum coherence.⁴⁴

C. Lineshape upon initial excitation into $|X_3\rangle$

Figure 7 demonstrates the positive SE/GSB cross-peak that reports the behavior of QD excited state population that is excited into $|X_3\rangle$ and subsequently relaxes into the band edge. As discussed previously, the growth of this feature reports on the relaxation of a hot electron through an Auger-like channel and subsequent relaxation of the corresponding hole through the valence band manifold to the band edge.^{21,59} For comparison, we plot the same metric reported in

Figures 5(b) and 5(c) for this feature in Figures 7(b) and 7(c). The SE/GSB shows minimal slope change over the first 1000 fs, identifying that size-dependent static disorder dominates the nonlinear response after initial excitation into $|X_3\rangle$. Because of the differential inhomogeneous broadening between two states as discussed previously, the model described in Eq. (1) predicts that the cross-peak between an initial state $|E_i\rangle$ and final state $|E_f\rangle$, located at spectral coordinates $\hbar\omega_\tau = E(|X_i\rangle)$ and $\hbar\omega_t = E(|X_f\rangle)$, should have a slope equal to $\Delta E_i/\Delta E_f$ if the nature of the coupling is size-dependent. The slope of this feature is ~ 0.5 , which matches the expected slope for size-dependent coupling, as described above ($\Delta E_1/\Delta E_3 = 0.5$). These results indicate that, during electron relaxation from P(e) to S(e), static disorder due to the size distribution of the QD sample strongly manifests itself in the photoresponse of QDs excited in this spectral region. 2DES resolves this size distribution within an ensemble along with the behavior of conduction band charge carriers.

D. Dynamics upon initial excitation into $|X_3\rangle$

The feature slope and position does not change during charge carrier relaxation; we therefore focus on the

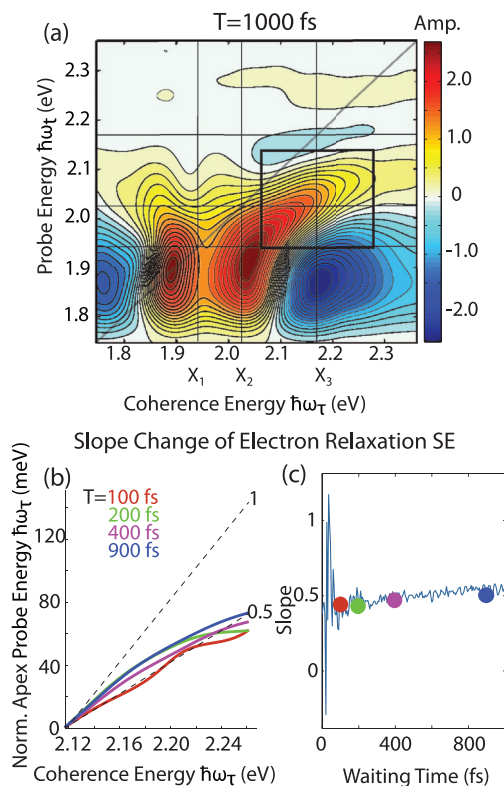


FIG. 7. (a) 2D spectrum of CdSe QDs taken at $T = 1000$ fs. (b) We plot the position of the vertical apex of the electron relaxation for several waiting times as described in the text. The change in the slope of this feature represents different processes that introduce static or dynamic disorder into the QD ensemble. To better show the change of slope, we subtract the minimum probe energy for each feature. (c) The feature plotted represents the cross-peak arising from hot electron relaxation and shows a constant slope of 0.5 across multiple population times, consistent with the ratio of size-dependent inhomogeneous broadening between $|X_3\rangle$ and $|X_1\rangle$.

amplitude change of this feature as a function of T in Figure 8. Figure 8(b) shows the amplitude of the feature apex for several specific points along the inhomogeneous bandwidth $|X_3\rangle/|X_1\rangle$ cross-peak as pictured in Figure 8(a). The trace follows a monoexponential decay with oscillations and noise modulating the signal. These oscillations are the subject of a separate paper⁴⁹ discussing coherent evolution of electronic and phonon states. After an initial large oscillatory period, the feature decays at different rates depending on initial excitation energy. Such inhomogeneous rates cannot be readily resolved by pump-probe spectroscopy; nonlinear methods such as Multiple Population Period Transient Spectroscopy (MUPPETS) have been designed specifically to probe such dynamics.^{77,78} Here, we use the echo effect in 2D spectroscopy to partially isolate different decay rates. In Figures 8(c) and 8(d), we observe that at higher excitation energies, the decay rate is significantly slower than it is at lower excitation energies, varying from 80 to 320 fs across the inhomogeneous bandwidth of the feature. We plot the decay rate across the ensemble in Figure 8(c). The center of the bandwidth (the peak of the $|X_3\rangle$ feature) decays at a rate of 167 fs, consistent with previous measures for dots of this size.^{21,59} However, at higher excitation energies, we observe slower relaxation, emphasized in Figure 8(c). This

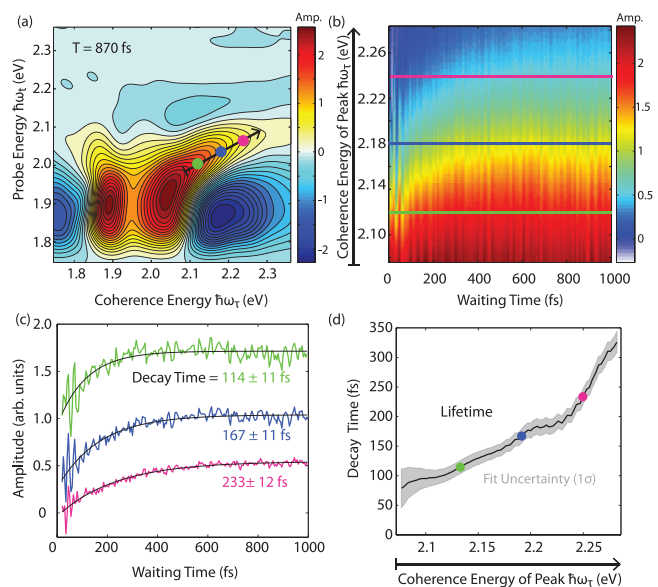


FIG. 8. (a) 2D spectrum taken at $T = 870$ fs, with the electron relaxation stimulated emission feature from which the amplitude relaxation is taken is highlighted with an arrow. (b) The waiting-time dynamics amplitude of the highlighted feature shown represented in part (a) with an arrow. To orient the reader, we show the same arrow on the y-axis. (c) Several color-coded traces representing waiting time charge-carrier relaxation, which are taken from colored points shown in (a), and highlighted in (b). As is shown, the dynamics vary across the feature, with center of the feature showing good agreement for electron relaxation measured for particles of this size. (d) The fit results are plotted across for all of the coherence input energies defined by the arrow in Figure (a), showing a range of relaxation time-scales across the bandwidth of the response. The error in each fit is represented by the gray shaded area.

trend runs counter to the trend expected for size alone. The red-edge of the feature represents large dots, while the blue-edge represents small dots within the polydisperse ensemble. As the charge-carrier Auger-like relaxation process suggests, smaller dots should show faster decay rates than larger dots, the opposite of the trend reported. We assign this discrepancy to multiple simultaneous relaxation processes; an Auger-like electron relaxation followed by hot hole relaxation to the band-edge state. In this way, while the average relaxation is size-dependent (in accordance previous TA work), “hotter” excitons in an ensemble will decay more slowly to the band-edge as they have to dissipate more energy. Thus, the rate of exciton relaxation varies both by state and by excitation within the state. In the future, analysis of different sized and more monodisperse QD preparations can help address this discrepancy.

IV. CONCLUSIONS

We demonstrate that C-2DES can complement TA studies, resolving inhomogeneous nonlinear response and charge-carrier relaxation. C-2DES provides context for TA measurements even in cases where the dynamics can be resolved with TA experiments. For example, in cases where the dynamics are highly heterogeneous, broadband TA, and even state-selective methods may integrate over multiple competing signals, resulting in complicated and perhaps contradictory results. In quantum dots, heterogeneity across the

ensemble makes 2DES an ideal method for resolving these signals, showing size-dependent heterogeneity (as seen in the $|X_3\rangle$ SE lineshape) and input energy dependent relaxation and solvation (such as the band-edge lineshape change, and $|X_3\rangle$ electronic relaxation). However, 2DES also has several drawbacks. For example, broadband excitation leads to convolved transient relaxation and coherent oscillations, adding significant uncertainty to estimates of timescales. Furthermore, the experiments require spectral and interferometric timing stability over longer acquisition times. In concert, both techniques can provide context and rigor to peak assignments not available separately.

In summary, C-2DES is used to examine the spectral signatures of charge carrier relaxation in semiconductor nanocrystals. We show that in colloidal QDs, we can resolve state-dependent effects on hot exciton cooling processes, showing signatures of differential surface trapping likelihood as a function of initial excitation. Furthermore, we show that the shape and position of the band-edge exciton shift as a result of dynamic interactions with the ligand/phonon bath as the exciton relaxes to the PL state on a ~ 330 fs time scale. In contrast, excitation into the hot-electron manifold shows size-dependent inhomogeneity in the peak shape of its nonlinear response. Finally, we illustrate differential rates in electron relaxation depending on initial excitation energy. These rates indicate that higher-energy excitation shows slower exciton cooling, within a specific excitonic state. These observations suggest that polydispersity and bath coupling can be used as independent tuning parameters for electron and hole behavior, respectively, when engineering novel QD technologies.

ACKNOWLEDGMENTS

The authors would like to thank National Science Foundation (NSF) MRSEC (Grant No. DMR 08-02054), The Keck Foundation, Packard Foundation, (U.S.) Department of Energy (DOE) Sunshot (DE-EE005312), (U.S.) Air Force Office of Scientific Research (USAFOSR) (Grant No. FA9550-09-1-0117), and DTRA (HDTRA1-10-1-0091) for supporting this work. J.R.C. and P.D.D. acknowledge support from the NSF GRFP. P.D.D. was supported in part by the Graduate Program in Biophysical Sciences at the University of Chicago (National Institutes of Health (NIH) Grant No. T32 EB009412).

¹A. P. Alivisatos, *J. Phys. Chem.* **100**, 13226 (1996).

²A. P. Alivisatos, *Science* **271**, 933 (1996).

³X. Michalet, F. F. Pinaud, L. A. Bentolila, J. M. Tsay, J. J. L. S. Doose, G. Sundaresan, A. M. Wu, S. S. Gambhir, and S. Weiss, *Science* **307**, 538 (2005).

⁴X. Gao, Y. Cui, R. M. Levenson, L. W. K. Chung, and S. Nie, *Nat. Biotechnol.* **22**, 969 (2004).

⁵M. Bruchez, M. Moronne, P. Gin, S. Weiss, and A. P. Alivisatos, *Science* **281**, 2013 (1998).

⁶J. A. Gupta, R. Knobel, N. Samarth, and D. D. Awschalom, *Science* **292**, 2458 (2001).

⁷A. Imamoglu, D. D. Awschalom, G. Burkard, D. P. DiVincenzo, D. Loss, M. Sherwin, and A. Small, *Phys. Rev. Lett.* **83**, 4204 (1999).

⁸B. O'Regan and M. Gratzel, *Nature (London)* **353**, 737 (1991).

⁹S. Coe-Sullivan, *Nat. Photon.* **3**, 315 (2009).

¹⁰V. I. Klimov, A. A. Mikhailovsky, S. Xu, A. Malko, J. A. Hollingsworth, C. A. Leatherdale, H.-J. Eisler, and M. G. Bawendi, *Science* **290**, 314 (2000).

¹¹Y. Kobayashi, T. Nishimura, H. Yamaguchi, and N. Tamai, *J. Phys. Chem. Lett.* **2**, 1051 (2011).

¹²F. R. Braakman, P. Barthelemy, C. Reichl, W. Wegscheider, and L. M. K. Vandersypen, *Nat. Nano* **8**, 432 (2013).

¹³S. A. Crooker, J. A. Hollingsworth, S. Tretiak, and V. I. Klimov, *Phys. Rev. Lett.* **89**, 186802 (2002).

¹⁴R. J. Ellingson, M. C. Beard, J. C. Johnson, P. Yu, O. I. Micic, A. J. Nozik, A. Shabaev, and A. L. Efros, *Nano Lett.* **5**, 865 (2005).

¹⁵R. D. Schaller, V. M. Agranovich, and V. I. Klimov, *Nat. Phys.* **1**, 189 (2005).

¹⁶M. C. Beard, K. P. Knutson, P. Yu, J. M. Luther, Q. Song, W. K. Metzger, R. J. Ellingson, and A. J. Nozik, *Nano Lett.* **7**, 2506 (2007).

¹⁷M. C. Beard, A. G. Midgett, M. C. Hanna, J. M. Luther, B. K. Hughes, and A. J. Nozik, *Nano Lett.* **10**, 3019 (2010).

¹⁸V. I. Klimov, *Annu. Rev. Phys. Chem.* **58**, 635 (2007).

¹⁹V. I. Klimov, *Science* **287**, 1011 (2000).

²⁰P. Kambhampati, *J. Phys. Chem. Lett.* **3**, 1182 (2012).

²¹P. Kambhampati, *J. Phys. Chem. C* **115**, 22089 (2011).

²²D. J. Norris, A. Sacra, C. B. Murray, and M. G. Bawendi, *Phys. Rev. Lett.* **72**, 2612 (1994).

²³D. J. Norris and M. G. Bawendi, *Phys. Rev. B* **53**, 16338 (1996).

²⁴E. A. McArthur, A. J. Morris-Cohen, K. E. Knowles, and E. A. Weiss, *J. Phys. Chem. B* **114**, 14514 (2010).

²⁵P. Kambhampati, *Acc. Chem. Res.* **44**, 1 (2010).

²⁶S. L. Sewall, R. R. Cooney, E. A. Dias, P. Tyagi, and P. Kambhampati, *Phys. Rev. B* **84**, 235304 (2011).

²⁷J. S. Kamal, A. Omari, K. Van Hoecke, Q. Zhao, A. Vantomme, F. Vanhaecke, R. K. Capek, and Z. Hens, *J. Phys. Chem. C* **116**, 5049 (2012).

²⁸S. L. Sewall, A. Franceschetti, R. R. Cooney, A. Zunger, and P. Kambhampati, *Phys. Rev. B* **80**, 081310 (2009).

²⁹P. A. Tekavec, K. L. M. Lewis, F. D. Fuller, J. A. Myers, and J. P. Ogilvie, *IEEE J. Sel. Top. Quantum Electron.* **18**, 210 (2012).

³⁰J. A. Myers, K. L. M. Lewis, F. D. Fuller, P. F. Tekavec, C. F. Yocom, and J. P. Ogilvie, *J. Phys. Chem. Lett.* **1**, 2774 (2010).

³¹M. Cho, *Chem. Rev.* **108**, 1331 (2008).

³²V. I. Klimov, D. W. McBranch, C. A. Leatherdale, and M. G. Bawendi, *Phys. Rev. B* **60**, 13740 (1999).

³³S. L. Sewall, R. R. Cooney, K. E. H. Anderson, E. A. Dias, D. M. Sagar, and P. Kambhampati, *J. Chem. Phys.* **129**, 084701 (2008).

³⁴K. E. Knowles, M. T. Frederick, D. B. Tice, A. J. Morris-Cohen, and E. A. Weiss, *J. Phys. Chem. Lett.* **3**, 18 (2011).

³⁵P. Guyot-Sionnest, M. Shim, C. Matranga, and M. Hines, *Phys. Rev. B* **60**, R2181 (1999).

³⁶A. Pandey and P. Guyot-Sionnest, *Science* **322**, 929 (2008).

³⁷G. Nair and M. G. Bawendi, *Phys. Rev. B* **76**, 081304 (2007).

³⁸J. M. Caruge, Y. Chan, V. Sundar, H. J. Eisler, and M. G. Bawendi, *Phys. Rev. B* **70**, 085316 (2004).

³⁹M. R. Salvador, M. A. Hines, and G. D. Scholes, *J. Chem. Phys.* **118**, 9380 (2003).

⁴⁰C. Y. Wong and G. D. Scholes, *J. Lumin.* **131**, 366 (2011).

⁴¹L. J. McKimmie, C. N. Lincoln, J. Jasieniak, and T. A. Smith, *J. Phys. Chem. C* **114**, 82 (2009).

⁴²A. P. Alivisatos, A. L. Harris, N. J. Levino, M. L. Steigerwald, and L. E. Brus, *J. Chem. Phys.* **89**, 4001 (1988).

⁴³E. Harel, S. M. Rupich, R. D. Schaller, D. V. Talapin, and G. S. Engel, *Phys. Rev. B* **86**, 075412 (2012).

⁴⁴D. B. Turner, Y. Hassan, and G. D. Scholes, *Nano Lett.* **12**, 880 (2011).

⁴⁵G. B. Griffin, S. Ithurria, D. S. Dolzhnikov, A. Linkin, D. V. Talapin, and G. S. Engel, *J. Chem. Phys.* **138**, 014705 (2013).

⁴⁶G. Moody, R. Singh, H. Li, I. A. Akimov, M. Bayer, D. Reuter, A. D. Wieck, A. S. Bracker, D. Gammon, and S. T. Cundiff, *Phys. Rev. B* **87**, 041304 (2013).

⁴⁷J. Seibt, T. Hansen, and T. Pullerits, *J. Phys. Chem. B* **117**, 11124 (2013).

⁴⁸J. Seibt and T. Pullerits, *J. Phys. Chem. C* **117**, 18728 (2013).

⁴⁹J. R. Caram, H. Zheng, P. D. Dahlberg, B. S. Rolczynski, G. B. Griffin, A. F. Fidler, D. S. Dolzhnikov, D. V. Talapin, and G. S. Engel, *J. Phys. Chem. Lett.* **5**, 196 (2013).

⁵⁰A. L. Efros and M. Rosen, *Annu. Rev. Mater. Sci.* **30**, 475 (2000).

⁵¹A. L. Efros and A. L. Efros, *Interband Absorption of Light in a Semiconductor Sphere* (Society of Photo-Optical Instrumentation Engineers, New York, 2005), Vol. 180.

- ⁵²See supplementary material at <http://dx.doi.org/10.1063/1.4865832> for figures and further discussion.
- ⁵³V. I. Klimov, *J. Phys. Chem. B* **104**, 6112 (2000).
- ⁵⁴O. Chen, X. Chen, Y. Yang, J. Lynch, H. Wu, J. Zhuang, and Y. C. Cao, *Angew. Chem., Int. Ed.* **47**, 8638 (2008).
- ⁵⁵V. Klimov, P. H. Bolivar, and H. Kurz, *Phys. Rev. B* **53**, 1463 (1996).
- ⁵⁶A. L. Efros, V. A. Kharchenko, and M. Rosen, *Solid State Commun.* **93**, 281 (1995).
- ⁵⁷D. Thomas and F. Michael, *Coherent Vibrational Dynamics* (CRC Press, 2007), p. 129.
- ⁵⁸D. M. Sagar, R. R. Cooney, S. L. Sewall, E. A. Dias, M. M. Barsan, I. S. Butler, and P. Kambhampati, *Phys. Rev. B* **77**, 235321 (2008).
- ⁵⁹V. I. Klimov and D. W. McBranch, *Phys. Rev. Lett.* **80**, 4028 (1998).
- ⁶⁰V. I. Klimov, *Nanocrystal Quantum Dots* (CRC Press, New York, 2010).
- ⁶¹V. P. Singh, A. F. Fidler, B. S. Rolczynski, and G. S. Engel, *J. Chem. Phys.* **139**, 084201 (2013).
- ⁶²J. Hybl, A. Albrecht, S. Faeder, and D. Jonas, *Chem. Phys. Lett.* **297**, 307 (1998).
- ⁶³D. M. Jonas, *Annu. Rev. Phys. Chem.* **54**, 425 (2003).
- ⁶⁴T. Brixner, T. Mančal, I. V. Stiopkin, and G. R. Fleming, *J. Chem. Phys.* **121**, 4221 (2004).
- ⁶⁵N. Krebs, I. Pugliesi, J. Hauer, and E. Riedle, *New J. Phys.* **15**, 085016 (2013).
- ⁶⁶N. Christensson, F. Milota, J. Hauer, J. Sperling, O. Bixner, A. Nemeth, and H. F. Kauffmann, *J. Phys. Chem. B* **115**, 5383 (2011).
- ⁶⁷V. V. Lozovoy, I. Pastirk, and M. Dantus, *Opt. Lett.* **29**, 775 (2004).
- ⁶⁸L. Lepetit, G. Chériaux, and M. Joffre, *J. Opt. Soc. Am. B* **12**, 2467 (1995).
- ⁶⁹T. Brixner, J. Stenger, H. M. Vaswani, M. Cho, R. E. Blankenship, and G. R. Fleming, *Nature (London)* **434**, 625 (2005).
- ⁷⁰G. Auböck, C. Consani, F. van Mourik, and M. Chergui, *Opt. Lett.* **37**, 2337 (2012).
- ⁷¹Y.-C. Cheng and G. R. Fleming, *J. Phys. Chem. A* **112**, 4254 (2008).
- ⁷²P. Guyot-Sionnest, E. Lhuillier, and H. Liu, *J. Chem. Phys.* **137**, 154704 (2012).
- ⁷³K. W. Stone, K. Gundogdu, D. B. Turner, X. Li, S. T. Cundiff, and K. A. Nelson, *Science* **324**, 1169 (2009).
- ⁷⁴J. I. Saari, E. A. Dias, D. Reifsnyder, M. M. Krause, B. R. Walsh, C. B. Murray, and P. Kambhampati, *J. Phys. Chem. B* **117**, 4412 (2012).
- ⁷⁵E. E. Fenn and M. D. Fayer, *J. Chem. Phys.* **135**, 074502 (2011).
- ⁷⁶V. I. Klimov, S. A. Ivanov, J. Nanda, M. Acherman, I. Bezel, J. A. McGuire, and A. Piryatinski, *Nature (London)* **447**, 441 (2007).
- ⁷⁷K. Sahu, H. Wu, and M. A. Berg, *J. Am. Chem. Soc.* **135**, 1002 (2013).
- ⁷⁸E. van Veldhoven, C. Khurmi, X. Zhang, and M. A. Berg, *ChemPhysChem* **8**, 1761 (2007).